Multibody System Dynamics
https://doi.org/10.1007/s11044-025-10089-7

RESEARCH

The influence of lever-propelled wheelchair parameters on locomotion performance: a predictive simulation study using a new equivalent muscle approach

Artur Fernando de Vito Jr.[1,2] · Fabrizio Leonardi[2] · Marko Ackermann[3,4]

Received: 23 December 2024 / Accepted: 14 June 2025

Abstract
Lever-propelled wheelchairs constitute a promising alternative to their handrim-propelled counterparts as they are associated with more favorable upper extremity biomechanics during propulsion. This can potentially reduce the large incidence of upper extremity pain and injury among long-term users of handrim-propelled wheelchairs. However, the effects of wheelchair design parameters on locomotion performance are poorly understood. Here, we propose a modeling approach and an optimal control framework to investigate the influence of parameters such as lever length, gear ratio, and position of the lever pivot on steady-state locomotion performance. We propose using a pair of equivalent antagonistic muscle units, called Equivalent Muscle Actuators (EMAs), acting directly on the propulsion levers and representing the intrinsic properties of the musculoskeletal system and its interaction with the device. This approach reduces the model dimension and promotes a straightforward analysis of the biomechanical advantage considering the human-device interaction. The predictive simulations of wheelchair locomotion are generated for various gear ratios and lever pivot positions at different average velocities, slope angles, and hand positions along the lever. The results reveal that a posterior pivot position requires consistently less effort due to a biomechanically more favorable configuration and gravity's beneficial effect during the propulsion phase. The results also indicate the most appropriate gear ratios depending on speed and slope angle. This study provides guidelines for the design of lever-propelled wheelchairs and a modeling and computational framework that can be extended to investigate different assistive technologies or other mechanical devices interacting with the human body.

Keywords Wheelchair locomotion · Lever-propelled wheelchairs · Predictive simulation · Musculoskeletal system modelling · Assistive technology

1 Introduction

Handrim-propelled wheelchairs are commonly used due to their simple design and low cost. This propulsion method, however, is inefficient and imposes repetitive loads on the upper extremities, leading to muscle fatigue, pain, and a high rate of injuries [1–4].

To improve the performance of wheelchair locomotion, alternative modes of propulsion have been proposed [5–7]. Particularly, the propulsion through levers has gained attention

Extended author information available on the last page of the article

as its advantages include reduced energy consumption and decreased muscle demand and joint loads on the upper extremity [5, 8–12]. Rütte et al. [12], for instance, show that the push-pull central-lever mechanism reduced peak forces exerted on the wheelchair by up to 40%, and energy consumption by up to 18% compared to handrim propulsion.

In common lever-propelled wheelchair designs, the lever is connected to the rear wheel by a roller chain or other power transmission systems attached to a ratchet and pawl mechanism or a one-way clutch that allows for torque transmission in only one direction. The easy repositioning results in a smoother and more continuous motion as the hand remains connected to the lever throughout the propulsion cycle [10]. Additionally, the hand can often be repositioned along the lever, providing a simple and effective way to adapt the overall mechanical advantage to different terrain conditions.

Given the potential benefits of lever propulsion, different studies have investigated how the design affects performance. For example, an experimental investigation indicated that more posterior pivot positions, closer to the rear wheel axle of the wheelchair, are more advantageous than more anterior ones [13]. The authors suggest that their findings could have practical implications for the design of lever-propelled wheelchairs and the training of athletes who use this type of propulsion. They note that a better understanding of the effects of lever design on performance could help optimize performance and reduce the risk of injury or fatigue during prolonged wheelchair use.

Sasaki et al. [10] researched the impact of the gear ratio of the lever propulsion mechanism on muscle effort and shoulder joint contact forces using a mechatronic simulator and a musculoskeletal model of the upper limb to estimate muscle and joint forces by inverse dynamics. The results show that a lever-propelled wheelchair with a 1.5 gear ratio led to lower cadence and shoulder contact forces compared to a conventional handrim-propelled wheelchair during level terrain locomotion. The effect of gear ratio on shoulder forces during lever-propelled locomotion was found to be large during uphill activities and at higher speeds. The authors suggest that further research is needed to determine the optimal design and technique for lever wheelchair propulsion that minimizes the risk of shoulder injuries or pain.

Predictive simulations using models of the musculoskeletal system are powerful tools to investigate wheelchair locomotion. These simulations can provide access to internal loads such as muscle and joint contact forces and allow systematic testing of design parameters before building physical prototypes. Fully predictive simulations based on optimal control frameworks, as used in this study, enable the investigation of a large number of locomotion scenarios without relying on experimental motion data [14–17]. Other simulation approaches based on tracking experimental kinematics or forces also contribute to understanding internal biomechanics during wheelchair propulsion [18, 19]. Recent applications of predictive simulation frameworks have also been proposed in the design and evaluation of wearable assistive devices such as ankle exoskeletons, supporting their potential to replicate energy and kinematic adaptations observed experimentally [20]. Forward dynamic simulations with detailed musculoskeletal models have also been used to explore handle-based propulsion strategies and their impact on muscle loading [21].

Recent studies have also used fully predictive optimal control simulations to explore manual wheelchair propulsion, highlighting the influence of configuration parameters such as anteroposterior stability on propulsion dynamics [22]. Predictive simulations provide the opportunity to test the effect of a large number of wheelchair configurations and design parameters before the prototype is built, potentially leading to effective designs and settings that reduce effort, improve comfort, and mitigate risk factors for injury, ultimately improving the quality of life of individuals with mobility impairments.

The generation of predictive simulations of human motion requires the solution of large-scale optimal control problems, which are particularly costly computationally due to the high dimensionality and complexity of the models involved [23]. Among the different strategies to address this challenge, model-reduction techniques can be applied to decrease the complexity and high dimensionality of musculoskeletal system models. Millard et al. [24], for example, presented a reduced musculoskeletal model that groups muscles into functional units, each represented by a single muscle comprising contractile and passive elements, referred to as a Muscle Torque Generator (MTG). Their findings demonstrated that this reduced model and a planar musculoskeletal framework accurately captured human movement dynamics with significantly lower computational costs compared to more intricate models. Bell et al. [25] extended the single Degree of Freedom (DoF) MTG to a 2-DoF MTG model for the shoulder joint, addressing the added complexity of joints with multiple degrees of freedom. By incorporating implicit coupling methods, they achieved accurate predictions of joint torques while maintaining computational efficiency. This type of reduced modeling approach was applied, for instance, to investigate optimal sports performance [26] and wheelchair locomotion [18].

Despite the potential of lever-propelled wheelchairs as an alternative to conventional handrim-propelled designs, there is limited understanding of this propulsion mode and its optimal design parameters. This study investigates how wheelchair design parameters — gear ratio, lever pivot positions, and hand position — affect locomotion performance across different velocities and slope angles using predictive simulations. In this work, performance is interpreted as neuromuscular effort and quantified through the time integral of squared actuator activations divided by the traveled distance over a complete cycle. To enable fully predictive simulations based on the solution of an optimal control problem, we adopted a reduced modeling approach in which the user's interaction with the system is represented by equivalent muscle-like actuators applying torque directly on the lever. This modeling choice reduces complexity and allows the simulation of multiple propulsion scenarios with varying mechanical configurations.

2 Methods

We propose an approach to model the effects of musculoskeletal system architecture and intrinsic muscle properties on lever-propelled wheelchair locomotion. The key concept is to implement a pair of antagonistic and agonistic Hill-type equivalent muscle units that act directly on the lever and represent the effect of a complex musculoskeletal Opensim model. This approach leads to a low-dimensional, continuous model that substantially reduces the computational cost to generate predictive simulations of wheelchair locomotion and unveils the combined effect of the musculoskeletal system and multibody system topology on task performance.

2.1 Multibody system model

The model assumes bilateral symmetry and comprises a planar closed kinematic chain with five rigid bodies: arms, forearms, levers, remaining body + wheelchair, and rear wheels, refer to Fig. 1. Ideal hinge joints are used to model the shoulder, elbow, lever pivot, wheelchair axle, and the connection between the hand and the lever. α represents the shoulder angle ($\alpha > 0$ for flexion) with respect to the trunk, which is assumed perpendicular to the ground. The elbow angle is denoted by β ($\beta > 0$ for flexion), while γ represents the angular position

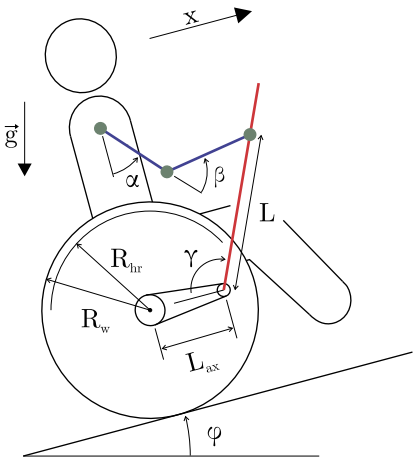

Fig. 1 Lever-propelled wheelchair model

Table 1 Mechanical parameters of the lever-propelled wheelchair model

Parameter	
Rear wheel radius	$R_w = 0.30\ m$
Handrim radius	$R_{hr} = 0.28\ m$
Rear wheel mass	$m_r = 3.0\ kg$
Rear wheel moment of inertia	$I_r = 0.28\ kg\,m^2$
Wheelchair mass	$m_c = 12.0\ kg$
Lever mass	$m_l = 0.8\ kg$
Lever moment of inertia	$I_r = 0.14\ kg\,m^2$

of the lever ($\gamma > 0$ for clockwise direction). The forward displacement of the wheelchair is represented by the coordinate x. The constant ground inclination with respect to the horizontal is described by φ.

The model has been adapted from the conventional wheelchair model as outlined in [16, 27], with the incorporation of the lever-based propulsion system and the introduction of the gear ratio (i_r) governing the relationship between lever and rear wheel rotations, defined as

$$i_r = \frac{\omega_w}{\dot{\gamma}}, \tag{1}$$

where ω_w represents the angular velocity of the rear wheel. The mechanical characteristics utilized in the computational simulations are detailed in Table 1.

The locomotion cycle is divided into two phases: the propulsion phase and the recovery phase. During the propulsion phase (indicated by subscript 1), the lever is coupled with the rear wheel through a fixed gear ratio, and the whole system has a single DoF. In this phase, the user exerts force on the lever, resulting in positive work being applied to the system. The equation of motion for this phase is formulated using the lever angle γ as the sole generalized coordinate as

$$q_1 = [\,\gamma_1\,]\,. \tag{2}$$

Conversely, during the recovery phase (indicated by subscript 2), the levers are decoupled from the rear wheels, and the mechanical system has two DoFs. The vector of generalized

coordinates $\boldsymbol{q_2}$ contains the lever angle γ and the coordinate x, which represents the displacement of the wheelchair, as

$$\boldsymbol{q_2} = [\,\gamma_2 \;\; x_2\,]^T\,. \tag{3}$$

Note that although the recovery phase has two degrees of freedom, the user's hand remains connected to the lever, and the closed kinematic chain is maintained.

The phases are defined by the instants $t_0 = 0$ at the beginning of the propulsion phase, t_1 at the transition between the propulsion and the recovery phase, and t_2 at the end of the recovery phase.

The equations of motion for the propulsion and recovery phases are derived symbolically using the Newton-Euler formalism in Matlab® as

$$M_1(q_1)\ddot{q}_1 + C_1(q_1, \dot{q}_1) = \tau_{ago} + \tau_{ant} + k_{g,1}(q_1) + k_{F,1}(F_r)\,, \tag{4}$$

$$\boldsymbol{M_2(q_2)\ddot{q}_2 + C_2(q_2, \dot{q}_2)} = \begin{bmatrix} \tau_{ago} + \tau_{ant} \\ 0 \end{bmatrix} + \boldsymbol{k_{g,2}(q_2)} + \boldsymbol{k_{F,2}}(F_r)\,, \tag{5}$$

where the index n indicates the phase, M_n are the mass matrices, C_n contains the Coriolis effects, τ_{ago} and τ_{ant} represent the muscle torques on the lever generated by the agonistic and antagonistic equivalent muscle units, respectively, $k_{g,n}$ are the generalized forces due to gravity forces, and $k_{F,n}$ are the generalized forces due to the rolling resistance force F_r (considered as 10 N per wheel as in [28]).

2.2 Equivalent muscle actuator

To reduce the dimensionality of musculoskeletal system models, which typically contain tens of muscles, each one with its own activation dynamics and intrinsic force-length-velocity properties, we introduce the idea of using equivalent muscles acting directly at the levers, called Equivalent Muscle Actuators (EMA). These actuators are conceived to represent the combined effect of all the muscles as seen from the wheelchair lever.

The approach is based on the fact that the kinematics of the four-bar mechanism encompassing the forearms, arms, levers, and body can be described using a single coordinate, conveniently selected in this study as the lever angle γ (Fig. 1). The virtual work produced by a pair of equivalent antagonistic and agonistic muscle units acting on the lever is equated to the virtual work of all muscles acting on the upper extremity of a large-scale OpenSim model. These equivalent muscle units represent the overall effect of the upper extremity muscle system on the lever, including the force-velocity and force-length relationships, as well as the activation dynamics. The EMAs allow us to characterize how much torque or mechanical work can be delivered by the user for different wheelchair configurations, while preserving essential features of neuromuscular behavior. This makes it possible to investigate how mechanical design influences the performance of the human-device system using predictive simulations without relying on motion tracking or predefined inputs.

The 3D OpenSim musculoskeletal model adopted in this study was developed by Chadwick et al. [29] and is available in https://simtk.org/projects/das. The model has 11 degrees of freedom, 138 muscle units (31 muscles), and seven distinct body parts (chest, collarbone, scapula, humerus, ulna, radius, and hand). The anthropometric data of the skeletal system, including body segment lengths, masses, and moments of inertia, were obtained from [30] to represent a person with a height of 1.70 m and a mass of 70 kg.

The first step to compute the equivalent muscle model is to determine the maximal force and the moment arms of the ith OpenSim muscle unit as a function of the lever's angular position γ and angular velocity $\dot{\gamma}$. These pieces of information can be extracted from the OpenSim model by performing numerical experiments for discrete values of the lever's angle and angular velocity, γ_j, and $\dot{\gamma}_k$. For each of these combinations, we compute the shoulder and elbow positions and velocities, $\alpha_{j,k}$, $\beta_{j,k}$, $\dot{\alpha}_{j,k}$, $\dot{\beta}_{j,k}$, by inverse kinematics in Matlab. The shoulder and elbow kinematics are fed into the OpenSim model, with all the other generalized coordinates fixed at their neutral positions so that the arm moves only in the sagittal plane. For each one of these numerical experiments, we extract finally the maximal forces $F_i^{max} = F_i^{max}(\gamma_j, \dot{\gamma}_k)$, and the moment arms with respect to the shoulder $\frac{\partial l_i}{\partial \alpha}(\gamma_j, \dot{\gamma}_k)$ and elbow $\frac{\partial l_i}{\partial \beta}(\gamma_j, \dot{\gamma}_k)$ for all muscles i from OpenSim, where l_i is the length of the ith muscle. The combinations of γ_j and $\dot{\gamma}_k$ were selected according to a 35×49 uniform grid. The range for γ_j is defined by a function that depends on the minimum angles the arm and forearm of the OpenSim model can reach, the position of the lever's center of rotation, and the lever length. The range for $\dot{\gamma}_k$ is set to $[-5\pi/3, 5\pi/3]\ rd/s$. This procedure is repeated for all investigated configurations, as explained further on. From now on, we omit the indices j and k for simplicity.

The maximal torque at the lever associated with the maximal force exerted by each muscle unit i can be computed using the principle of virtual work as a function of lever position and velocity as

$$\tau_i^{max}(\gamma, \dot{\gamma}) = \frac{\partial l_i}{\partial \gamma} F_i^{max}(\gamma, \dot{\gamma}) \tag{6}$$

where ${}^{\partial l_i}/_{\partial \gamma}$ can be interpreted as the moment arm of the ith muscle unit with respect to the lever's center of rotation and be further decomposed using the multi-variable chain rule as

$$\lambda_i \triangleq \frac{\partial l_i}{\partial \gamma} = \frac{\partial l_i}{\partial \alpha}\frac{\partial \alpha}{\partial \gamma} + \frac{\partial l_i}{\partial \beta}\frac{\partial \beta}{\partial \gamma}\,. \tag{7}$$

The moment arms of muscle i with respect to the shoulder, ${}^{\partial l_i}/_{\partial \alpha}$, and elbow, ${}^{\partial l_i}/_{\partial \beta}$, are known from the musculoskeletal model, while ${}^{\partial \alpha}/_{\partial \gamma}$, and ${}^{\partial \beta}/_{\partial \gamma}$ are kinematic relationships associated with the closed-loop, four-bar kinematic chain (Fig. 1).

The effect of all muscles on the lever will now be represented by a pair of equivalent muscles acting directly on the lever, an agonistic equivalent muscle pulling the lever forward and applying positive work to the system when the lever moves forward, and an antagonistic one, pulling the lever backward. Since F_i^{max} is always positive in Equation (6), the sign of λ_i in Equation (7) determines whether muscle i exerts positive power ($\lambda_i > 0$) or negative power ($\lambda_i < 0$) when lever velocity $\dot{\gamma}$ is positive. Therefore, the maximal torque of the equivalent agonistic ago and antagonistic ant muscles can be computed, respectively, as

$$\tau_{ago}^{max}(\gamma, \dot{\gamma}) = \sum_{i=1}^{N} \max(0, \lambda_i) F_i^{max}(\gamma, \dot{\gamma})\,, \tag{8}$$

$$\tau_{ant}^{max}(\gamma, \dot{\gamma}) = \sum_{i=1}^{N} \min(\lambda_i, 0) F_i^{max}(\gamma, \dot{\gamma})\,, \tag{9}$$

where N is the number of muscle units in the original OpenSim model.

To represent the overall level of muscle recruitment, an activation level a ranging from 0 to 1 is introduced for each equivalent muscle so that the resulting torques are obtained by

$$\tau_{ago}(\gamma, \dot{\gamma}) = a_{ago}\tau_{ago}^{max}(\gamma, \dot{\gamma}), \tag{10}$$

$$\tau_{ant}(\gamma, \dot{\gamma}) = a_{ant}\tau_{ant}^{max}(\gamma, \dot{\gamma}). \tag{11}$$

The muscle activation dynamics, reflecting the fact the muscles are not ideal actuators and that there is a lag between neural command and muscle force response, are modeled by first-order differential equations [31, 32] as

$$\frac{d\,a_{ago}}{d\,t} = \left(u_{ago} - a_{ago}\right)\left(\frac{u_{ago}}{T_{act}} + \frac{1 - u_{ago}}{T_{deact}}\right), \tag{12}$$

$$\frac{d\,a_{ant}}{d\,t} = \left(u_{ant} - a_{ant}\right)\left(\frac{u_{ant}}{T_{act}} + \frac{1 - u_{ant}}{T_{deact}}\right), \tag{13}$$

where u_{ago} and u_{ant} are the overall neural excitations of the agonistic and antagonistic equivalent muscles, ranging from 0 to 1 and representing the system controls, and T_{act} and T_{deact} are activation and deactivation time constants. We adopt $T_{act} = 10$ ms and $T_{deact} = 40$ ms, which are consistent with values reported in the literature [33].

The approach proposed in this section reduces the complex high-dimensional OpenSim model to a much simpler one (Equations (10) to (13)) composed of only two equivalent muscle units incorporating the intrinsic properties of the whole musculoskeletal system and its interaction with the wheelchair.

2.3 Optimal control problem formulation

After defining the two equivalent muscles and their activation dynamics, as presented in the previous section, this section outlines the formulation of the predictive simulation framework. The predictive simulations are obtained by solving a two-phase optimal control problem (OCP), Equations (14)-(24), consisting of searching for the states (generalized coordinates, generalized velocities, and muscle activations), controls (neural excitations), and phase durations that minimize the quadratic objective function

$$J_c = \frac{1}{t_2\bar{v}}\left(\int_0^{t_1}\left(u_{ago}^2 + u_{ant}^2\right)dt + \int_{t_1}^{t_2}\left(u_{ago}^2 + u_{ant}^2\right)dt\right), \tag{14}$$

where t_1 is the time instant representing the end of the propulsion phase and the beginning of the recovery phase, t_2 is the final time of the cycle, and $\bar{v}$ is the prescribed average locomotion velocity. This cost function, referred to as neuromuscular effort, represents the integration of effort over the locomotion cycle divided by the distance traveled in a cycle (corresponding to $t_2\bar{v}$). It enables the comparison across different locomotion velocities, analogous to metabolic cost of transport, a performance criterion frequently used in experimental evaluation and predictive simulation of locomotion with mobility assistive devices.

The OCP is subject to a set of constraints, including the equations of motion presented in Equations (4) and (5), governing the dynamics during the propulsion and recovery phases,

respectively, and the activation dynamics in Equations (12) and (13), with activation and neural excitation bounded by 0 to 1, as

$$0 \leq a_{ago}, u_{ago}, a_{ant}, u_{ant} \leq 1\,. \tag{15}$$

The durations of the propulsion and recovery phases were treated as free optimization variables in the optimization, with lower and upper bounds set, respectively, to 0.1 s and 3 s for each phase. In the propulsion phase, a positive angular velocity for the lever ($\dot{\gamma}_1 > 0$) is ensured. During the recovery phase, the angular velocity of the lever is constrained to remain lower than the angular velocity of the rear wheel after reduction, thereby preventing the coupling between the lever and the rear wheel as

$$\dot{\gamma}_2 \leq \dot{x}\, i_r\, R_w\,. \tag{16}$$

The phase transition constraints include the requirement that the position of the wheelchair at the beginning of the return phase $x_2(t_1)$ is equal to the distance traveled during the propulsion phase,

$$x_2(t_1) = (\gamma_1(t_1) - \gamma_1(0))\, i_r\, R_w\,, \tag{17}$$

and that the velocity at the beginning of the return phase $\dot{x}_2(t_1)$ is equal to the velocity at the end of the propulsion phase,

$$\dot{x}_2(t_1) = \dot{\gamma}_1(t_1)\, i_r\, R_w\,. \tag{18}$$

Moreover, a continuous transition between the propulsion and the recovery phases requires

$$\gamma_1(t_1) = \gamma_2(t_1)\,, \tag{19}$$

$$\dot{\gamma}_1(t_1) = \dot{\gamma}_2(t_1)\,, \tag{20}$$

and a periodic motion with a collisionless transition between the recovery and the propulsion phases requires

$$\gamma_2(t_2) = \gamma_1(0)\,, \tag{21}$$

$$\dot{\gamma}_2(t_2) = \dot{\gamma}_1(0)\,. \tag{22}$$

Additionally, lower and upper bounds on shoulder and elbow angles are added according to the reference model proposed by [29] as

$$\begin{aligned} \alpha_{min} \leq \alpha(\gamma) \leq \alpha_{max}\,, \\ \beta_{min} \leq \beta(\gamma) \leq \beta_{max}\,. \end{aligned} \tag{23}$$

Finally, a prescribed average locomotion velocity $\bar{v}$ is imposed with

$$x_2(t_2) = \bar{v}\, t_2\,. \tag{24}$$

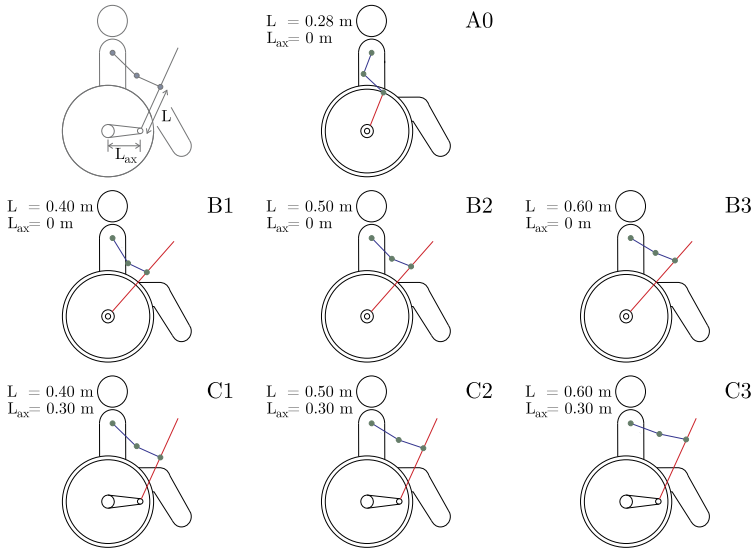

Fig. 2 Illustration of the seven investigated configurations, where L is the distance of the hand position with respect to the pivot along the lever, and L_{ax} is the horizontal position of the lever's pivot with respect to the rear wheel axis

2.4 Simulations

A distinctive feature of lever-propelled wheelchairs is the possibility of moving the hand along the lever, changing the lever arm (L) with respect to the pivot, as illustrated in Fig. 1. Additionally, the pivot can be constructively installed in different locations with respect to the rear-wheel axle, represented as L_{ax} in Fig. 1. In this investigation, we explore combinations of lever arm L and pivot position L_{ax}, which compose 7 configurations as illustrated in Fig. 2.

In Group A, containing a single configuration A0, the lever's center of rotation coincides with the rear-wheel axis, and the hand distance to the pivot is the same as the handrim radius, with $L = R_{hr}$. This condition approximates handrim-propelled wheelchair locomotion. Although the trajectory of the hand in the recovery phase is constrained along the handrim, we consider this configuration close enough to handrim-propelled locomotion to serve as a reference for comparison. In this group, the lever's mass and moment of inertia were set to 0 kg to approximate it to handrim-propelled locomotion further.

In Group B, the lever's center of rotation is positioned at the center of the rear wheel, while in Group C, it is offset by 0.3 m to the front. Both groups, B and C, have three configurations corresponding to three different hand positions along the lever, with $L =$ 0.4 m, $L = 0.5$ m, and $L = 0.6$ m. These values were selected based on previous studies on lever-propelled wheelchairs: $L = 0.42$ m [10], $L = 0.49$ m [34], and $0.395 < L < 0.480$ m [13].

For each of the seven configurations in Fig. 2, the effect of different transmission ratios i_r (Equation (1)) is investigated at different locomotion speeds, on a level surface, and a constant slope. Eight gear ratios, ranging from 0.5 to 2.25, with increments of 0.25, were tested. On a level surface ($\varphi = 0°$ in Fig. 1), average velocities of $\bar{v} = 0.5$ m/s, 1.0 m/s, and 1.5 m/s were simulated. For locomotion on a slope with $\varphi = 4°$, the velocity was fixed

at $\bar{v} = 0.5$ m/s. This resulted in 168 combinations for locomotion on a level surface (7 configurations $\times$ 8 gear ratios $\times$ 3 velocities) and 56 combinations for locomotion on the slope (7 configurations $\times$ 8 gear ratios), totalizing 224 simulations.

The OCP was solved using the PROPT® software, which implements a Direct Collocation approach. The mesh employed was determined through a sensitivity assessment with respect to the number of collocation points and the objective function value. Beyond 50 collocation points per phase, the objective function exhibits minimal variation. Therefore, the simulations were generated with 51 collocation points per phase, resulting in 102 collocation points in a cycle.

To obtain the optimal control problem solutions for locomotion on the horizontal plane, we first solved the optimal control problem for a velocity of 0.1 m/s. The simulations for higher velocities were obtained from this initial solution by sequentially increasing the velocity by 0.1 m/s until 1.5 m/s, using the previously obtained solution as the initial guess for the next velocity. For the locomotion on a slope, the simulations were obtained according to the following strategy:

1. From an initial guess corresponding to the locomotion on the horizontal plane at 0.5 m/s, solve the optimization problem for a slope of 1° and a velocity of 0.1 m/s.
2. From this solution, obtain the solution for larger velocities sequentially with increments of 0.1 m/s until 0.5 m/s.
3. From the solution for 0.5 m/s and slope of 1°, obtain solutions for higher inclinations with increments of 1° until the maximal slope angle of 4° is achieved.

This strategy was repeated for each combination of hand position, pivot position, and gear ratio. This approach improves convergence and ensures consistency across multiple configurations, but does not systematically search for or guarantee global optimality. The optimization problems were solved using SNOPT's default convergence settings, with a feasibility tolerance of 10^{-6} and an optimality tolerance of 10^{-6}.

3 Results

The proposed equivalent model and implemented optimal control approach allowed the generation of the 224 simulations in approximately two hours and 29 minutes on a computer with an Intel i7 processor and 32 GB of RAM. Each simulation took approximately 40 seconds of CPU time on average. It is important to note that the time required for curve generation for each of the seven configurations is not included in this stage, as these are calculated only once. As an illustration of typical predicted patterns, Fig. 3 shows the muscle activation and kinematics results obtained for locomotion on a level surface with configuration B2, average velocity $\bar{v} = 1.0$ m/s, and gear ratio $i_r = 1.75$. In the propulsion phase ($0\% - 29.7\%$ of the cycle), the agonistic equivalent muscle is activated (Fig. 3.a), applying positive work and accelerating the wheelchair forward (Fig. 3.b), while the lever moves clockwise, the shoulder moves counterclockwise, and the elbow extends (Fig. 3.c). The activation of the antagonistic muscle and the decoupling of the lever and rear wheel characterize the start of the recovery phase (29.7%). The lever is first decelerated until it reaches zero angular velocity and the furthest position from the trunk ($29.7\% - 39.2\%$). Subsequently, the lever is accelerated backward under the continuing effect of the antagonistic muscle until its deactivation and the reactivation of the agonistic muscle ($39.2\% - 66.1\%$). This reactivation of the agonistic muscle decelerates the backward motion of the lever until it reaches zero angular velocity and the nearest position to the trunk ($66.1\% - 90\%$). Finally, under the continuing

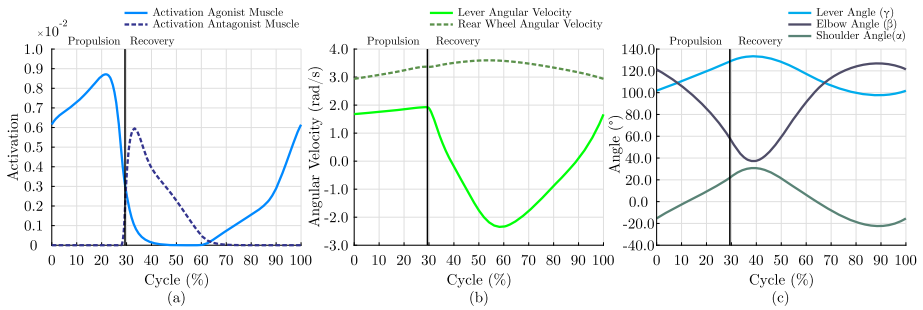

Fig. 3 Predicted equivalent muscle activations (a), kinematics (b), and joint angles (c) for locomotion on a level surface with configuration B2, average velocity $\bar{v} = 1.0$ m/s, and gear ratio $i_r = 1.75$ (Color figure online)

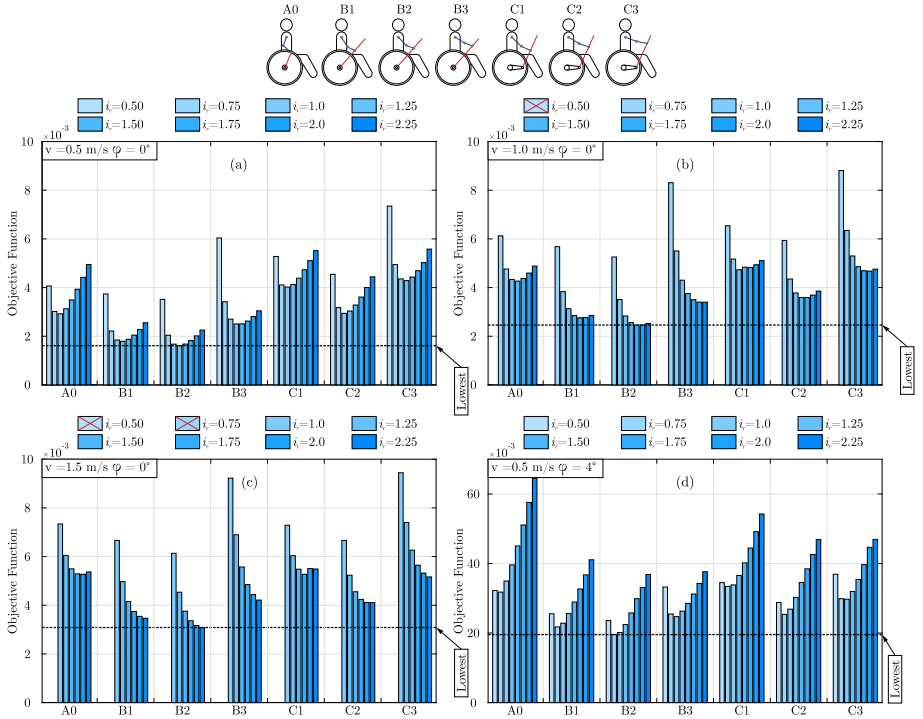

Fig. 4 Predicted locomotion performance for different lever-propelled wheelchair configurations. Each bar represents the cost function value for one configuration defined by hand position, pivot location, and gear ratio (illustrated at the top). Results are shown for four conditions: (a) $\bar{v} = 0.5$ m/s, $\varphi = 0°$, (b) $\bar{v} = 1.0$ m/s, $\varphi = 0°$, (c) $\bar{v} = 1.5$ m/s, $\varphi = 0°$, and (d) $\bar{v} = 0.5$ m/s, $\varphi = 4°$ (Color figure online)

effect of the agonistic muscle, the lever is accelerated until it reaches the coupling velocity (90% − 100%), and the cycle is restarted.

The results show that the different configurations and gear ratios can substantially affect the locomotion performance in terms of the cost function value (Figs. 4(a), (b), (c) and (d)).

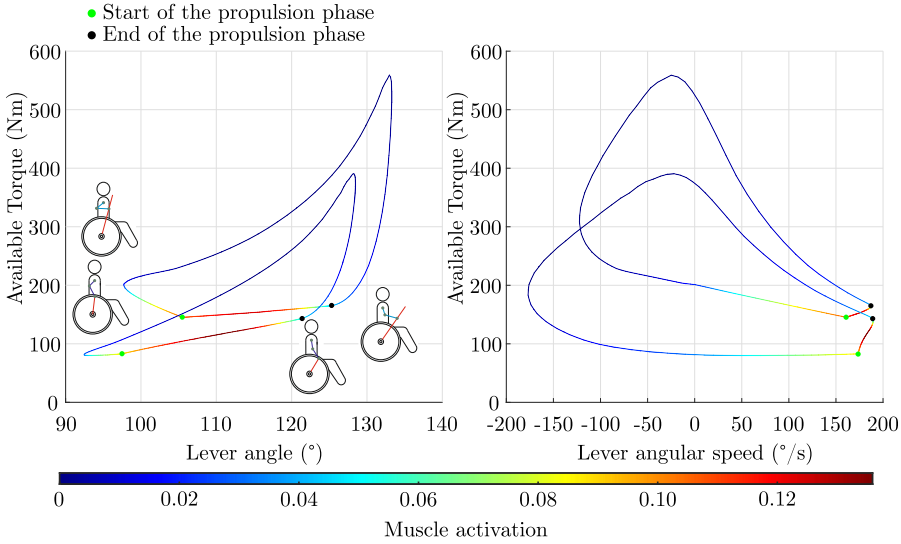

Fig. 5 Available torque along the propulsion cycle by the equivalent agonistic muscle *ago* with respect to the lever angle (left) and lever's angular velocity (right) for locomotion on a level surface with an average velocity of $\bar{v}$ =1.0 m/s, and a gear ratio of $i_r = 1$ for conditions A0 and B2. The color map indicates muscle activation intensity (Color figure online)

For all investigated conditions (locomotion velocities and terrain inclination), it is clear that the B configurations, with the lever pivot coincident with the rear wheel axis, outperform the reference A0 configuration representing handrim-propelled wheelchairs. Shifting the handle forward, as in configuration group C, deteriorated the performance, leading to comparable or worse cost function values than the A0 ones.

At lower gear ratios, no convergence was observed as the locomotion velocity increased. Specifically, at a velocity of 1.0 m/s, the simulation failed to converge for a gear ratio of $i_r = 0.5$. Likewise, at a velocity of 1.5 m/s, the simulation did not converge for gear ratios of $i_r = 0.5$ and $i_r = 0.75$. These combinations of higher locomotion velocities and lower gear ratios lead to increased upper body velocities and accelerations, leading to large inertial forces that surpass the available muscle capacity, which is diminished due to the torque-velocity relationship.

Regarding hand position along the lever, a distance of $L = 0.5$ m generally led to lower effort compared to higher or lower values of L for both configuration groups (B2 and C2) and all conditions.

Optimal gear ratios, in turn, increase with locomotion speed. The best performing configuration B2 presented its lowest cost function values at gear ratios $i_r = 1.25$, $i_r = 1.75$, and $i_r = 2.25$, at velocities $\bar{v} = 0.5$ m/s, $\bar{v} = 1.0$ m/s and $\bar{v} = 1.5$ m/s, respectively. For the locomotion on a 4°-slope at 0.5 m/s (Fig. 4d), the optimal gear ratios are lower, as expected, ranging from $i_r = 0.75$ to $i_r = 1.00$.

The proposed equivalent muscle approach led to a low computational cost, allowing a straightforward analysis and interpretation of the results. In particular, this approach unveiled how different design configurations affect the biomechanical performance of the user-wheelchair system. Figures 5 and 6 illustrate this by comparing configuration B2 to configurations A0 and C2, respectively. The plots display the available torque capacity of the agonistic EMA over the full simulated propulsion cycle as a function of simulated lever

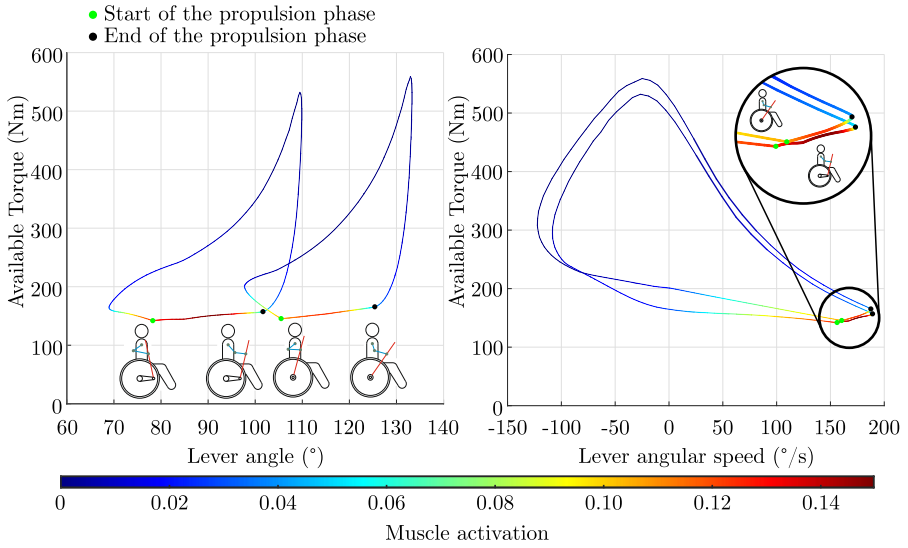

Fig. 6 Available torque along the propulsion cycle by the equivalent agonistic muscle *ago* with respect to the lever angle (left) and lever's angular velocity (right) for locomotion on a level surface with an average velocity of $\bar{v}$ =1.0 m/s, and a gear ratio of $i_r = 1$ for conditions B2 and C2. The color map indicates muscle activation intensity (Color figure online)

angle (left) and angular velocity (right), evidencing the underlying force—length—velocity relationship. The color code indicates the predicted normalized neural excitation, representing the fraction of the available torque applied by the agonistic EMA in the simulation. Note that the region of low available torque coincides with the propulsion phase as muscles apply force concentrically (with reduced force capacity), and the mechanical gain is less favorable (with arms more flexed). This, associated with the fact that larger forces are required in the propulsion phase, leads to larger activation levels (indicated in red). Conversely, the part of the cycle with negative lever velocity corresponds to conditions in which this agonistic EMA would contract eccentrically and apply negative work, which are the reasons for higher muscle capacity and low activation (indicated in blue), respectively.

Figure 5 shows a substantially larger torque capacity of configuration B2 compared to A0, evidencing the biomechanical advantage provided by the lever-propelled wheelchair compared to a conventional handrim-propelled wheelchair. B2 provides a biomechanical advantage also with respect to C2, albeit less evident in the propulsion phase, as shown in Fig. 6. In this case, the superior performance of B2 can also be explained by the positive effect of gravity in the propulsion phase. To better understand this effect, Fig. 7 presents the generalized torque acting on the lever due to gravity, as defined in Equation (4). Configuration B2 exhibits consistently higher generalized gravitational torque – approximately 6 N m more than C2 – throughout the propulsion phase. This difference arises from the posterior positioning of the lever pivot in B2, which leads to a forward leaning of the lever and the beneficial effect of gravity during the propulsion phase. As a result, part of the required net torque is provided by gravity, reducing the effort demanded from the agonistic actuator.

Figure 8 shows the cadence (in cycles per second) for configurations A0 and B2 across varying gear ratios (i_r), locomotion velocities ($v = 0.5$, 1.0, 1.5 m/s), and terrain inclinations (slope $= 0°$ and $4°$). For each condition, cadence decreased as gear ratio increased, consistent with the expected inverse relationship between cadence and mechanical advantage.

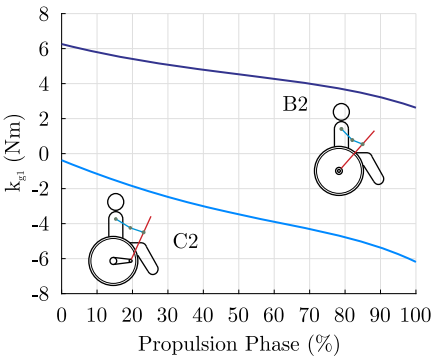

Fig. 7 Generalized torque due to gravity at the lever along the propulsion phase $k_{g1}(q_1)$ as in Equation (4) for locomotion on a level surface with an average velocity of $\bar{v} = 1.0$ m/s, and gear ratio $i_r = 1$ for conditions B2 and C2 (Color figure online)

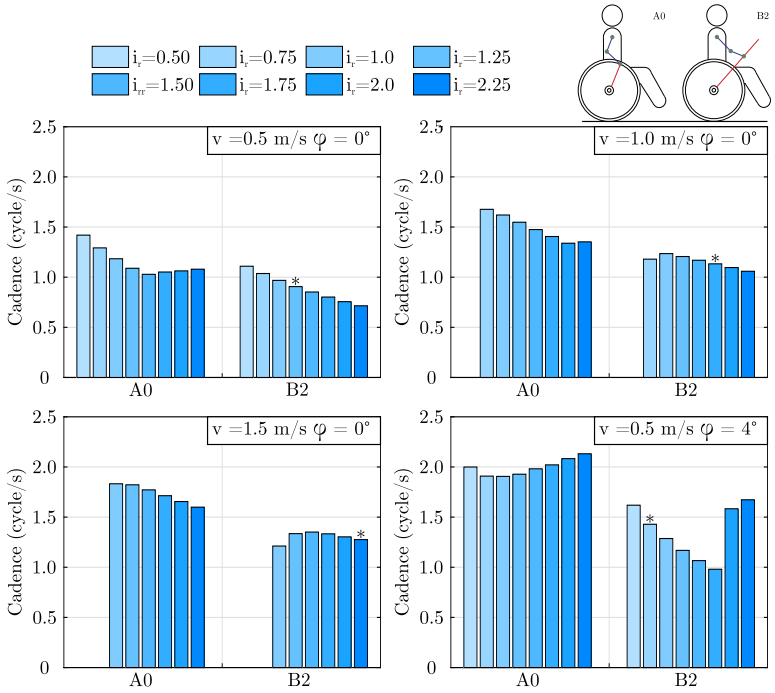

Fig. 8 Predicted cadence (cycles/s) for configuration A0 and B2. Conditions marked with $*$ indicate the optimal condition in terms of effort (14), employed as the objective function for generating the predictive simulation (Color figure online)

Across all scenarios, configuration B2 exhibited lower cadence values than A0, especially at higher velocities, which reflects the effect of the longer stroke length associated with lever propulsion. Conditions marked with an asterisk indicate the configurations with the lowest cost function value among the tested cases.

To complement the cadence results, Tables 6 to 9 present the predicted duty cycle values across all valid simulations. In general, lever-propelled configurations tend to operate with lower duty cycles than A0 across all conditions, indicating shorter propulsion phase dura-

tions as a fraction of the complete cycle duration. It can also be observed that the duty cycle increases with increasing gear ratios and decreases with increasing velocity.

4 Discussion

The use of MTGs is a common model-reduction approach to decrease model dimension and computation cost in predictive simulations of human motion [16, 18, 24]. The proposed modeling approach in this study extends the idea of MTGs to cases where the human musculoskeletal system interacts with a mechanical device, such as a robot, mobility assistive aid, sports equipment, or machine, with the formation of one-DoF closed kinematic chains. We show that these model topologies allow the use of a single pair of antagonistic torque generators, acting directly onto the mechanical system. This pair of equivalent actuators, called EMAs, represents not only the intrinsic muscle system properties but also the effect of the multibody system configuration, containing device and human body segments. Besides lever-propelled wheelchair locomotion [12], other examples of potential applications of this approach are in modeling of walking with crutches [35], canoeing [36], and rowing [37].

EMAs can be derived from complex musculoskeletal models, as in this study, from biological joint MTGs, or through experimental measurements of the resulting generalized torque during maximal voluntary contraction at different combinations of the corresponding generalized coordinate and generalized velocity.

One possible advantage of EMAs over MTGs is the potential for further model reduction. A single pair of EMAs is required for each one-DoF kinematic chain instead of a pair of MTGs for each active biological joint in the kinematic chain. In this study, for instance, instead of a single pair of EMAs, two pairs of MTGs, one pair at the shoulder and another one at the elbow, would be required, increasing the dimension of the problem and potentially leading to higher computational cost to solve the associated large-scale optimal control problem. Another interesting feature of EMAs is the intrinsic incorporation of the combined effect of biarticular muscles. This is a limitation of MTGs as they are derived for individual joints independently and, therefore, cannot take into account the combined effect of adjacent joint angular velocities and positions on the force generation capacity of biarticular muscles. However, these potential benefits were not systematically investigated here, and the present discussion is speculative. A systematic comparison between EMA and MTG formulations, in terms of computational performance, accuracy, and biomechanical interpretability, remains a relevant direction for future work.

Finally, and not least importantly, EMAs are a powerful tool for unveiling and interpreting the overall available actuation capacity of the human body, considering the musculoskeletal properties and kinematic constraints resulting from the human-device interaction. As evidenced in this study, a single pair of EMAs acting directly on the levers could represent the equivalent effect of all upper limb muscles and associated mechanical gains, providing a straightforward interpretation of the reason for the superiority of one system configuration over another. EMAs, therefore, can be a useful tool during the design process by providing deeper insight into the human-device interaction.

The advantages of EMAs come at the expense of fewer actuation degrees of freedom. The approach relies on a single equivalent neural excitation for each of the antagonistic EMAs, modulating the maximal torque-velocity-position relationships. This single neural excitation per EMA can oversimplify the muscle recruitment patterns, a limitation that is shared with the MTGs. Another important limitation of the approach is that the closed kinematic

chain needs to have a single degree of freedom. An extension of the approach to kinematic chains with more than one degree of freedom may be possible but will require further assumptions on how equivalent actuators are defined and distributed. EMAs are problem- and configuration-specific. In fact, we needed to derive a different pair of EMAs for each hand position along the lever, as this changes the parameters of the closed-loop kinematic chain. This is a clear disadvantage compared to MTGs, which do not change depending on the device and how the person interacts with it. Furthermore, because the actuator moment is applied directly to the lever, this formulation does not allow the estimation of internal or interaction forces between the user and the device (e.g., individual muscle forces, joint contact forces, hand forces), which limits direct comparison with experimental data.

While limited in scope, the results align with prior studies indicating potential biomechanical benefits of lever-propelled wheelchairs relative to handrim-based configurations [8, 10, 13, 34]. Jolanta et al. [34], for instance, show that the physiological metrics VO2max, heart rate, and ventilation were significantly lower during lever-propelled locomotion compared to handrim-propelled locomotion, indicating that it was less physically demanding, particularly at higher speeds. In our study, the cost function values (Figs. 4(a), (b), (c), (d)) for lever-propelled wheelchair locomotion (configurations B and C) are consistently lower than the ones for handrim-propelled wheelchair (configuration A) for the tested scenarios, except for locomotion on an even surface at $\bar{v} = 0.5$ m/s with configuration C (Fig. 4a). This evidences that lever-propelled wheelchairs are mostly advantageous, but poor design choices in gear ratios, pivot location, and hand misplacement along the lever can deteriorate performance, even canceling out the gains over handrim-propelled wheelchairs.

The comparison of available torque in the agonistic EMAs in Fig. 5 reveals that the better performance of lever-propelled wheelchairs (configuration B2) compared to handrim-propelled wheelchairs (configuration A0) is due to a substantial biomechanical and mechanism configuration advantage. Indeed, the available torque of the agonistic EMA in B2 exceeds the one in A0 by 20% to over 100% in the critical propulsion phase and the preceding acceleration phase, leading to lower overall muscle excitation and the observed reduced effort.

The results show that the position of the lever's pivot plays an important role in performance, with posterior placement (configuration B) presenting substantially superior performance compared to an anterior one (configuration C) in all tested scenarios (Figs. 4(a), (b), (c), (d)). This finding corroborates previous literature reports indicating that a posterior placement enhances performance. Fiok et al. [13], for instance, designed a dedicated test bench to assess various lever configurations, including adjustable lever lengths and axis positions, and concluded that placing the pivot close to the rear wheel axis improves performance based on measurements of heart rate, mechanical efficiency, and surface EMG.

The proposed modeling approach unveils the causes for the better performance of posteriorly located lever pivots. The comparison of the available torque by the agonistic EMA in conditions B2 and C2 in Fig. 6 evidences the biomechanical advantage of B2 over C2, particularly in the acceleration phase preceding the propulsion phase. This difference, however, does not fully explain the substantial difference in performance observed in Fig. 4b. A deeper analysis reveals that the generalized torque due to gravity during the propulsion phase also contributes significantly to the reduction of muscle activations during this critical phase, as evidenced in Fig. 7. This favorable gravitational effect on the mechanisms with posterior pivot positions in the propulsion phase is associated with an unfavorable effect on the recovery phase. However, as the recovery phase is uncritical, presenting low activation levels, the overall effect of gravity on the effort over the complete cycle is beneficial.

The results also show an important effect of gear ratio on performance. As expected, smaller gear ratios i_r (low gear) performed better at low speeds and slopes, while performance at increasing speeds requires progressively larger gear ratios (high gear). It is noteworthy that a gear ratio of $i_r = 1.0$ is close to optimal at a lower speed of $\bar{v} = 0.5$ m/s on a level surface as well as on a steep 4° slope and performs satisfactorily at $\bar{v} = 1.0$ m/s. The fact that this speed range is commonly encountered in most daily activities, combined with the finding that placing the lever pivot on the rear wheel axis is favorable, supports the conclusion that a simple mechanical design can result in highly effective wheelchairs. A design featuring a gear ratio of $i_r = 1.0$ and a lever pivot attached to the rear wheel axis via a ratcheting mechanism eliminates the need for complex mechanical transmission systems.

However, users who require locomotion at higher speeds over longer distances would certainly benefit from higher gear ratios, according to the simulation results. More complex designs may be justified in these cases, with variable gear ratios or fixed higher gear ratios determined by a trade-off between performance at lower and higher velocities.

While the position of the hand along the handle affects the overall mechanical gain, interacting to some extent with the gear ratio, its most important influence is on upper extremity configuration and the resulting biomechanical characteristics of the resulting EMAs, changing the equivalent torque capacity and available range of motion. A position of the hand corresponding to $L = 0.5$ m was shown to be consistently favorable in all investigated scenarios. This could be a general guideline for the placement of anatomical handles on the lever. However, allowing for fine-tuned hand position adjustment along the lever might be interesting, depending on the user's anthropometrics and terrain conditions.

Propulsion cadence is related to the frequency of periodic loading on the upper extremity and is considered a relevant aspect in the evaluation of wheelchair locomotion [10]. Although cadence was not included in the cost function, the resulting values from simulations minimizing effort can be observed in Fig. 8, comparing the handrim-propelled configuration A0 with the lever-propelled configuration B2. While configuration A0 was used as a baseline to represent handrim-propelled locomotion, we acknowledge that it only reproduces an "arcing" pattern in the recovery phase — a strategy that can be biomechanically less efficient than other hand trajectories in the recovery phase [38]. Therefore, using A0 as a reference scenario may underestimate the performance potential of optimized handrim propulsion, even considering that the impact is expected to be small because the recovery phase is associated with substantially lower muscle activity than the propulsion phase. Accordingly, the advantages of lever-propelled configurations observed in our simulations should be interpreted in light of this modeling choice. Further investigation comparing lever propulsion with more efficient handrim propulsion patterns is needed to better contextualize these findings.

The simulated cadence for the A0 configuration at a target velocity of 1.0 m/s was approximately 1.5 Hz, which is higher than values typically reported in the literature for handrim-propelled wheelchair locomotion. For instance, Boninger et al. [39] reported an average cadence of 1.13 Hz with a standard deviation of 0.18 Hz for the arcing pattern (propulsion speed of 0.90 m/s). Similarly, Rankin et al. [40] evaluated four propulsion strategies: (i) self-selected, (ii) maximum contact angle, (iii) minimum peak force, and (iv) minimum cadence. Propulsion velocity and cadence varied according to the adopted strategy. The following values represent the means across subjects, with standard deviations shown in parentheses: (i) 1.11 (0.24) m/s, 0.83 (0.17) Hz; (ii) 1.06 (0.20) m/s, 0.48 (0.18) Hz; (iii) 1.00 (0.18) m/s, 1.04 (0.21) Hz; and (iv) 1.06 (0.23) m/s, 0.27 (0.13) Hz. These findings indicate that the propulsion strategy can substantially affect cadence, and suggest that the high cadence observed in our A0 simulations may be partially attributed to the absence of

cadence-related penalization in the cost function or to limitations inherent to the reduced modeling approach.

Although the results presented here are consistent with existing literature and previous experimental studies, the analysis remains speculative to a certain extent, and future experimental validation is required. Future studies should consider the effect of different body anthropometry, motor control limitations, fore-aft adjustment of rear wheel position with respect to the shoulder, as well as different model assumptions. The adopted model assumes the trunk does not move with respect to the wheelchair and that the motion is contained in the sagittal plane. Also, during acceleration periods and in slopes, there exists the possibility of a pitch motion of the wheelchair, which we have not considered in our simulations. The performance of these different configurations should also be evaluated in curves and transient conditions beyond steady-state locomotion along a straight trajectory. Furthermore, the problem could be reformulated to include some of the parameters, such as the gear ratio, as optimization variables within the OCP, allowing for the identification of task-dependent optimal settings, and complementing the parametric analysis conducted here.

One important limitation of the proposed framework is that it does not provide direct access to standard biomechanical indicators such as joint torques, shoulder contact forces, or energy expenditure estimates that are commonly used in experimental studies. The EMA formulation was intentionally designed to reduce model complexity and enable predictive simulations across many configurations, but this comes at the cost of biomechanical resolution. While trends in neuromuscular effort may qualitatively align with metrics like heart rate and metabolic cost, the present framework does not allow direct estimation of physiological or joint-level loads. A potential direction for future work is to post-process the kinematic and kinetic outputs of the predictive simulations using a full musculoskeletal model, such as the original OpenSim model used to construct the EMA surfaces. This would include, for instance, the application of inverse dynamics or muscle-driven simulations to estimate joint torques and reaction forces from the patterns predicted by the OCP with the simplified model. Such a hybrid approach could combine the scalability of the OCP+EMA framework with the biomechanical detail provided by anatomically accurate models.

Another limitation concerns the wrist joint, which was considered as an unactuated hinge joint connected directly to the lever. For the specific task of lever propulsion, we assumed that the wrist torque has a limited influence on net torque transmission to the lever. This simplification is common in the literature for similar tasks (e.g., [14, 16, 18]), where focus is placed on shoulder and elbow contributions. Nevertheless, in tasks such as handrim propulsion, wrist moments, particularly on the ulnar and radial deviation directions, can influence the effective force generation capacity.

The discussed limitations evidence the future need for experimental validation. To this end, different lever-propelled wheelchair locomotion can be experimentally investigated using a motorized treadmill under prescribed velocity and slope conditions in a motion capture laboratory to collect kinematics and temporal parameters. The force applied to the lever can be collected using a custom instrumented lever. Additionally, metabolic energy expenditure could be estimated based on oxygen consumption. This would provide a powerful experimental setup to validate our modelling approach and to investigate the effect of design parameters on lever-propelled wheelchair locomotion.

5 Conclusions

The analysis presented in this study is exploratory in nature and focuses on evaluating specific, mechanically plausible configurations of lever-propelled wheelchairs on locomotion

performance across various velocities and terrain slopes using predictive simulations. The proposed Equivalent Muscle Actuator (EMA) acts directly on the device and represents the combined effect of the muscle system and the closed kinematic chain configuration, leading to a substantial model reduction while providing insights into the human-device interaction. The predictive simulations show a clear advantage of lever-propelled over conventional handrim-propelled wheelchairs in terms of required effort and propulsion cadence if the design parameters are chosen appropriately. The results also show that the placement of the lever's pivot on the rear wheel's axis is advantageous compared to a more anterior position and that a 1:1 gear ratio leads to a nearly optimal performance for low velocities and satisfactory performance for moderate velocities. These combined findings indicate that the simplest mechanical design, with the lever attached directly to the rear wheel's axis and no additional transmission, is an effective solution for activities of daily living, leading to a reliable and affordable design. A design with higher or variable gear ratios seems to be only justified for more active users, requiring locomotion at higher velocities. Furthermore, a hand placed at 0.5 m from the axis along the lever was shown to lead consistently to better performance, which provides another relevant design guideline. Although the predicted performance is consistent with existing experimental findings in the literature, the developed lever-propelled wheelchair model is not fully validated, and the reported conclusions remain speculative to some extent, requiring future experimental confirmation.

Appendix

Table 2 Objective function for $\bar{v} = 0.5$ m/s, and slope = 0°. Cells are color-coded from green to red according to the value of the objective function: lower values are closer to green, and higher values are closer to red (Color table online)

Configuration	ir=0.5	0.75	1	1.25	1.5	1.75	2	2.25
A0	0.00407	0.00302	0.00292	0.00313	0.00349	0.00393	0.00442	0.00495
B1	0.00374	0.00222	0.00185	0.00179	0.00188	0.00205	0.00228	0.00255
B2	0.00352	0.00204	0.00168	0.00161	0.00168	0.00182	0.00202	0.00225
B3	0.00604	0.00342	0.00270	0.00250	0.00251	0.00262	0.00281	0.00304
C1	0.00528	0.00411	0.00402	0.00412	0.00439	0.00473	0.00511	0.00552
C2	0.00454	0.00318	0.00294	0.00304	0.00328	0.00361	0.00400	0.00444
C3	0.00735	0.00494	0.00436	0.00429	0.00443	0.00469	0.00502	0.00558

Table 3 Objective function for $\bar{v} = 1.0$ m/s, and slope = 0°. Cells are color-coded from green to red according to the value of the objective function: lower values are closer to green, and higher values are closer to red (Color table online)

Configuration	ir=0.5	0.75	1	1.25	1.5	1.75	2	2.25
A0	NA	0.00612	0.00476	0.00434	0.00427	0.00438	0.00460	0.00488
B1	NA	0.00568	0.00383	0.00313	0.00285	0.00275	0.00277	0.00286
B2	NA	0.00526	0.00351	0.00283	0.00256	0.00246	0.00246	0.00253
B3	NA	0.00831	0.00551	0.00430	0.00375	0.00350	0.00340	0.00340
C1	NA	0.00654	0.00517	0.00473	0.00484	0.00483	0.00493	0.00511
C2	NA	0.00593	0.00435	0.00378	0.00359	0.00359	0.00369	0.00386
C3	NA	0.00881	0.00635	0.00530	0.00485	0.00469	0.00468	0.00476

Table 4 Objective function for $\bar{v} = 1.5$ m/s, and slope = 0°. Cells are color-coded from green to red according to the value of the objective function: lower values are closer to green, and higher values are closer to red (Color table online)

Configuration	ir=0.5	0.75	1	1.25	1.5	1.75	2	2.25
A0	NA	NA	0.00734	0.00605	0.00550	0.00529	0.00527	0.00537
B1	NA	NA	0.00667	0.00497	0.00415	0.00374	0.00354	0.00347
B2	NA	NA	0.00613	0.00454	0.00376	0.00336	0.00317	0.00308
B3	NA	NA	0.00922	0.00690	0.00557	0.00485	0.00444	0.00421
C1	NA	NA	0.00729	0.00604	0.00548	0.00527	0.00551	0.00549
C2	NA	NA	0.00666	0.00523	0.00456	0.00424	0.00412	0.00411
C3	NA	NA	0.00945	0.00740	0.00626	0.00565	0.00532	0.00517

Table 5 Objective function for $\bar{v} = 0.5$ m/s, and slope = 4°. Cells are color-coded from green to red according to the value of the objective function: lower values are closer to green, and higher values are closer to red (Color table online)

Configuration	ir=0.5	0.75	1	1.25	1.5	1.75	2	2.25
A0	0.0322	0.0318	0.0350	0.0396	0.0451	0.0511	0.0576	0.0645
B1	0.0255	0.0218	0.0228	0.0256	0.0289	0.0327	0.0367	0.0411
B2	0.0236	0.0196	0.0201	0.0225	0.0258	0.0299	0.0331	0.0369
B3	0.0332	0.0255	0.0247	0.0263	0.0285	0.0312	0.0343	0.0376
C1	0.0345	0.0334	0.0339	0.0366	0.0402	0.0445	0.0492	0.0542
C2	0.0288	0.0254	0.0269	0.0303	0.0345	0.0385	0.0426	0.0469
C3	0.0369	0.0299	0.0297	0.0319	0.0354	0.0397	0.0447	0.0469

Table 6 Duty cycle for $\bar{v} = 0.5$ m/s, and slope = 0°. Cells are color-coded from green to red according to the value of the duty cycle: lower values are closer to green, and higher values are closer to red (Color table online)

Configuration	ir=0.5	0.75	1	1.25	1.5	1.75	2	2.25
A0	0.179	0.291	0.390	0.472	0.534	0.566	0.596	0.620
B1	0.135	0.225	0.312	0.390	0.458	0.516	0.565	0.607
B2	0.129	0.213	0.295	0.371	0.437	0.494	0.544	0.586
B3	0.100	0.170	0.243	0.313	0.377	0.434	0.485	0.530
C1	0.173	0.282	0.298	0.366	0.422	0.461	0.488	0.516
C2	0.127	0.210	0.292	0.367	0.433	0.492	0.541	0.585
C3	0.094	0.162	0.231	0.299	0.362	0.419	0.470	0.448

Table 7 Duty cycle for $\bar{v} = 1.0$ m/s, and slope = 0°. Cells are color-coded from green to red according to the value of the duty cycle: lower values are closer to green, and higher values are closer to red (Color table online)

Configuration	ir=0.5	0.75	1	1.25	1.5	1.75	2	2.25
A0	NA	0.142	0.212	0.280	0.343	0.400	0.451	0.482
B1	NA	0.096	0.150	0.206	0.261	0.313	0.362	0.407
B2	NA	0.088	0.139	0.191	0.243	0.294	0.341	0.385
B3	NA	0.062	0.108	0.153	0.199	0.244	0.288	0.329
C1	NA	0.119	0.191	0.260	0.253	0.300	0.343	0.380
C2	NA	0.085	0.135	0.186	0.238	0.289	0.336	0.381
C3	NA	0.061	0.101	0.146	0.190	0.234	0.277	0.318

Table 8 Duty cycle for $\bar{v} = 1.5$ m/s, and slope = 0°. Cells are color-coded from green to red according to the value of the duty cycle: lower values are closer to green, and higher values are closer to red (Color table online)

Configuration	ir=0.5	0.75	1	1.25	1.5	1.75	2	2.25
A0	NA	NA	0.136	0.190	0.242	0.292	0.339	0.383
B1	NA	NA	0.087	0.129	0.170	0.212	0.254	0.294
B2	NA	NA	0.078	0.118	0.157	0.196	0.235	0.274
B3	NA	NA	0.052	0.088	0.124	0.159	0.194	0.228
C1	NA	NA	0.110	0.163	0.218	0.269	0.249	0.285
C2	NA	NA	0.077	0.113	0.152	0.191	0.231	0.269
C3	NA	NA	0.052	0.085	0.119	0.152	0.186	0.220

Table 9 Duty cycle for $\bar{v} = 0.5$ m/s, and slope = 4°. Cells are color-coded from green to red according to the value of the duty cycle: lower values are closer to green, and higher values are closer to red (Color table online)

Configuration	ir=0.5	0.75	1	1.25	1.5	1.75	2	2.25
A0	0.334	0.443	0.516	0.566	0.602	0.630	0.652	0.670
B1	0.276	0.397	0.497	0.551	0.586	0.614	0.636	0.651
B2	0.267	0.381	0.477	0.555	0.619	0.670	0.621	0.638
B3	0.232	0.338	0.432	0.496	0.525	0.556	0.584	0.608
C1	0.371	0.499	0.449	0.499	0.541	0.576	0.602	0.624
C2	0.278	0.392	0.488	0.560	0.607	0.579	0.600	0.620
C3	0.231	0.333	0.426	0.504	0.570	0.624	0.669	0.588

Acknowledgements This work was developed thanks to the financial support of CAPES (Coordination for the Improvement of Higher Education Personnel), Program PDPG 88887.940152/2024-00.

Author contributions A.F.V.Jr and M.A. conceived the study. A.F.V.Jr performed simulations, analyzed the data, and wrote the main manuscript. F.A. and M.A. supervised the work and revised the manuscript and provided additional input. All authors read and approved the final manuscript.

Funding information Open Access funding enabled and organized by Projekt DEAL.

Data availability The Matlab code used in this work and animations are available at https://github.com/arturvito/Optimal-Control-of-Lever-Propelled-Wheelchair-Locomotion.

Declarations

Competing interests The authors declare no competing interests.

References

1. Curtis, K.L., Tyner, T., Zachary, L., Lentell, G.L., Brink, D., Didyk, T.V., Gean, K., Hall, J.H., Hooper, M., Klos, J., Lesina, S., Pacillas, B.: Effect of a standard exercise protocol on shoulder pain in long-term wheelchair users. Spinal Cord **37**, 421–429 (1999). https://doi.org/10.1038/sj.sc.3100860
2. van der Woude, L.H.V., Veeger, H.E.J., Dallmeijer, A.J., Janssen, T.W.J., Rozendaal, L.A.: Biomechanics and physiology in active manual wheelchair propulsion. Med. Eng. Phys. **23**(10), 713–733 (2001). https://doi.org/10.1016/S1350-4533(01)00083-2
3. Richter, W.M.: The effect of seat position on manual wheelchair propulsion biomechanics: a quasi-static model-based approach. Med. Eng. Phys. **23**(10), 707–712 (2001). https://doi.org/10.1016/S1350-4533(01)00074-1
4. Heyward, O., Vegter, R., Groot, S., Woude, L.V.D.: Shoulder complaints in wheelchair athletes: a systematic review. PLoS ONE **12**, e0188410 (2017). https://doi.org/10.1371/journal.pone.0188410
5. Woude, L.H.V., Dallmeijer, A.J., Janssen, T.W.J., Veeger, D.: Alternative modes of manual wheelchair ambulation: an overview. Am. J. Phys. Med. Rehabil. **80**(10), 765–777 (2001). https://doi.org/10.1097/00002060-200110000-00012
6. Sarraj, A.R., Massarelli, R.: Design history and advantages of a new lever-propelled wheelchair prototype. Int. J. Adv. Robot. Syst. **8**(3), 26 (2011). https://doi.org/10.5772/10669
7. Lui, J., MacGillivray, M., Sheel, A.W., Jeyasurya, J., Sadeghi, M., Sawatzky, B.: Mechanical efficiency of two commercial lever-propulsion mechanisms for manual wheelchair locomotion. J. Rehabil. Res. Dev. **50**(10), 1363–1372 (2013). https://doi.org/10.1682/JRRD.2013.02.0034
8. Woude, L.H.V., Veeger, H.E.J., Boer, Y.A., Rozendal, R.H.: Physiological evaluation of a newly designed lever mechanism for wheelchairs. J. Med. Eng. Technol. **17**(6), 232–240 (1993). https://doi.org/10.3109/03091909309006331
9. Requejo, P.S., Lee, S.E., Mulroy, S.J., Haubert, L.L., Bontrager, E.L., Gronley, J.K., Perry, J.: Shoulder muscular demand during lever-activated vs pushrim wheelchair propulsion in persons with spinal cord injury. J. Spinal Cord Med. **31**(5), 568–577 (2008). https://doi.org/10.1080/10790268.2008.11754604
10. Sasaki, M., Stefanov, D., Ota, Y., Miura, H., Nakayama, A.: Shoulder joint contact force during lever-propelled wheelchair propulsion. ROBOMECH J. **2**(1), 13 (2015). https://doi.org/10.1186/s40648-015-0037-8
11. Marszałek, J., Kosmol, A., Mróz, A., Wiszomirska, I., Fiok, K., Molik, B.: Physiological parameters depending on two different types of manual wheelchair propulsion. Assist. Technol. **32**, 229–235 (2018). https://doi.org/10.1080/10400435.2018.1529005
12. Rütte, T.A., Trigo, F., Bessems, L., Woude, L.H.V., Vegter, R.J.K.: A novel push-pull central-lever mechanism reduces peak forces and energy-cost compared to hand-rim wheelchair propulsion during a controlled lab-based experiment. J. NeuroEng. Rehabil. **19**(1), 30 (2022). https://doi.org/10.1186/s12984-022-01007-5
13. Fiok, K., Mróz, A.: How does lever length and the position of its axis of rotation influence human performance during lever wheelchair propulsion? J. Electromyogr. Kinesiol. **25**(5), 824–832 (2015). https://doi.org/10.1016/j.jelekin.2015.06.007
14. Cuerva, V.I., Ackermann, M., Leonardi, F.: The influence of speed and slope angle on wheelchair propulsion patterns: an optimal control study. In: 24th ABCM International Congress of Mechanical Engineering, p. 1154 (2017). https://doi.org/10.26678/ABCM.COBEM2017.COB17-1154
15. Laschowski, B., Mehrabi, N., McPhee, J.: Optimization-based motor control of a paralympic wheelchair athlete. Sports Eng. **21**, 207–215 (2018). https://doi.org/10.1007/s12283-018-0265-2
16. Cuerva, V.I., Ackermann, M., Leonardi, F.: Performance of impedance control-based strategies in power-assisted wheelchairs: a predictive simulation study. Front. Neurorobot. **16**, 805835 (2022). https://doi.org/10.3389/fnbot.2022.805835
17. Loisel, J., Rouvier, T., Hybois, S., Bascou, J., Sauret, C.: Optimal control formulation for manual wheelchair locomotion simulations: influence of anteroposterior stability. J. Biomech. Eng. **145**(11), 111012 (2023). https://doi.org/10.1115/1.4063274. https://asmedigitalcollection.asme.org/biomechanical/article-pdf/145/11/111012/7040234/bio_145_11_111012.pdf
18. Brown, C., McPhee, J.: Predictive forward dynamic simulation of manual wheelchair propulsion on a rolling dynamometer. J. Biomech. Eng. **142**(7), 071008 (2020). https://doi.org/10.1115/1.4046298
19. Walford, S.L., Rankin, J.W., Mulroy, S.J., Neptune, R.R.: Differences in glenohumeral joint contact forces between recovery hand patterns during wheelchair propulsion with and without shoulder muscle weakness: a simulation study. J. Biomech. Eng. **146**(4), 041005 (2024). https://doi.org/10.1115/1.4064590
20. Ganesan, K., Gupta, A.: Predictive simulation framework for replicating energy reduction trends and joint kinematic adaptations in walking with powered ankle exoskeletons. Multibody Syst. Dyn. (2024). https://doi.org/10.1007/s11044-024-10040-2

21. Kurup, N.B.R., Puchinger, M., Gföhler, M.: Forward dynamic optimization of handle path and muscle activity for handle based isokinetic wheelchair propulsion: a simulation study. Comput. Methods Biomech. Biomed. Eng. **22**(1), 55–63 (2019). https://doi.org/10.1080/10255842.2018.1527321
22. Loisel, J., Rouvier, T., Hybois, S., Bascou, J., Sauret, C.: Optimal control formulation for manual wheelchair locomotion simulations: influence of anteroposterior stability. J. Biomech. Eng. **145**(11), 111012 (2023). https://doi.org/10.1115/1.4063274
23. Ackermann, M., Bogert, A.J.: Optimality principles for model-based prediction of human gait. J. Biomech. **43**(6), 1055–1060 (2010). https://doi.org/10.1016/j.jbiomech.2009.12.012
24. Millard, M., Emonds, A.L., Harant, M., Mombaur, K.: A reduced muscle model and planar musculoskeletal model fit for the simulation of whole-body movements. J. Biomech. **89**, 11–20 (2019). https://doi.org/10.1016/j.jbiomech.2019.04.004
25. Bell, S., Nasr, A., McPhee, J.: General muscle torque generator model for a two degree-of-freedom shoulder joint. J. Biomech. Eng. **146**(8), 081008 (2024). https://doi.org/10.1115/1.4065044
26. Inkol, K.A., Brown, C., McNally, W., Jansen, C., McPhee, J.: Muscle torque generators in multibody dynamic simulations of optimal sports performance. Multibody Syst. Dyn. **50**(4), 435–452 (2020). https://doi.org/10.1007/s11044-020-09747-9
27. Ackermann, M., Leonardi, F., Costa, H.R., Fleury, A.T.: Modeling and optimal control formulation for manual wheelchair locomotion: the influence of mass and slope on performance. In: 5th IEEE RAS/EMBS International Conference on Biomedical Robotics and Biomechatronics, pp. 1079–1084 (2014). https://doi.org/10.1109/BIOROB.2014.6913924
28. Woude, L., Geurts, C., Winkelman, H., Veeger, H.: Measurement of wheelchair rolling resistance with a handle bar push technique. J. Med. Eng. Technol. **27**(6), 249–258 (2003). https://doi.org/10.1080/0309190031000096630
29. Chadwick, E.K., Blana, D., Kirsch, R.F., Bogert, A.J.: Real-time simulation of three-dimensional shoulder girdle and arm dynamics. IEEE Trans. Biomed. Eng. **61**, 1947–1956 (2014). https://doi.org/10.1109/TBME.2014.2309727
30. Winter, D.A.: Biomechanics and Motor Control of Human Movement, 4th edn. Wiley, Chichester (2009). https://doi.org/10.1002/9780470549148
31. He, J., Levine, W.S., Loeb, G.E.: Feedback gains for correcting small perturbations to standing posture. IEEE Trans. Autom. Control **36**(3), 322–332 (1991). https://doi.org/10.1109/9.73565
32. Delp, S.L., Anderson, F.C., Arnold, A.S., Loan, P., Habib, A., John, C.T., Guendelman, E., Thelen, D.G.: Opensim: open-source software to create and analyze dynamic simulations of movement. IEEE Trans. Biomed. Eng. **54**(11), 1940–1950 (2007). https://doi.org/10.1109/TBME.2007.901024
33. Millard, M., Uchida, T., Seth, A., Delp, S.L.: Flexing computational muscle: modeling and simulation of musculotendon dynamics. J. Biomech. Eng. **135**, 021005 (2013). https://doi.org/10.1115/1.4023390
34. Marszałek, J., Kosmol, A., Mróz, A., Wiszomirska, I., Fiok, K., Molik, B.: Physiological parameters depending on two different types of manual wheelchair propulsion. Assist. Technol. **32**(5), 229–235 (2020). https://doi.org/10.1080/10400435.2018.1529005
35. Febrer-Nafría, M., Pallarès-López, R., Fregly, B.J., Font-Llagunes, J.M.: Prediction of three-dimensional crutch walking patterns using a torque-driven model. Multibody Syst. Dyn. **51**(1), 1–19 (2020). https://doi.org/10.1007/s11044-020-09751-z
36. Liu, L., Qiu, S., Wang, Z., Li, J., Wang, J.: Canoeing motion tracking and analysis via multi-sensors fusion. Sensors **20**(7), 2110 (2020). https://doi.org/10.3390/s20072110
37. Smith, R.M., Loschner, C.: Biomechanics feedback for rowing. J. Sports Sci. **20**(10), 783–791 (2010). https://doi.org/10.1080/026404102320675639
38. Slowik, J.S., Requejo, P.S., Mulroy, S.J., Neptune, R.R.: The influence of wheelchair propulsion hand pattern on upper extremity muscle power and stress. J. Biomech. **49**(9), 1554–1561 (2016). https://doi.org/10.1016/j.jbiomech.2016.03.031
39. Boninger, M.L., Souza, A.L., Cooper, R.A., Fitzgerald, S.G., Koontz, A.M., Fay, B.T.: Propulsion patterns and pushrim biomechanics in manual wheelchair propulsion. Arch. Phys. Med. Rehabil. **83**(5), 718–723 (2002). https://doi.org/10.1053/apmr.2002.32455
40. Rankin, J.W., Kwarciak, A.M., Richter, W.M., Neptune, R.R.: The influence of wheelchair propulsion technique on upper extremity muscle demand: a simulation study. Clin. Biomech. **27**(9), 879–886 (2012). https://doi.org/10.1016/j.clinbiomech.2012.07.002

Authors and Affiliations

Artur Fernando de Vito Jr.[1,2] · Fabrizio Leonardi[2] · Marko Ackermann[3,4]

✉ M. Ackermann
marko.ackermann@kit.edu

A.F. de Vito Jr.
arturfvj@unicamp.br

F. Leonardi
fabrizio@fei.edu.br

1 School of Applied Sciences, University of Campinas, Limeira, Brazil

2 Department of Mechanical Engineering, Centro Universitário FEI, Sao Bernardo do Campo, Brazil

3 Institute for Anthropomatics and Robotics (IAR), Karlsruhe Institute of Technology (KIT), Karlsruhe, Germany

4 Institute of Computer Engineering, Heidelberg University, Heidelberg, Germany